ELECTRONIC SUPPORTING INFORMATION

Spin Crossover Polysaccharide Nanocomposites

Alexey Tokarev,[a] Jérôme Long,[a] Yannick Guari,*[a] Joulia Larionova,[a] Françoise Quignard,[b] Pierre Agulhon,[b] Mike Robitzer,[b] Gábor Molnár,[c] Lionel Salmon,[c] Azzedine Bousseksou*[c].

[a]*Institut Charles Gerhardt, UMR 5253, Chimie Moléculaire et Organisation du Solide, Université Montpellier II, Place E. Bataillon, 34095 Montpellier cedex 5, France*

[b]*Institut Charles Gerhardt, UMR 5253 CNRS-UM2-ENSCM-UM1, Matériaux Avancés pour la Catalyse et la Santé, ENSCM, 8 rue de l'Ecole Normale, 34296 Montpellier cedex 5, France*

[c] *Laboratoire de Chimie de Coordination, CNRS & Université de Toulouse (UPS, INP), 31077 Toulouse, France*

* Corresponding authors. E-mail: Azzedine.bousseksou@lcc-toulouse.fr, yannick.guari@univ-montp2.fr

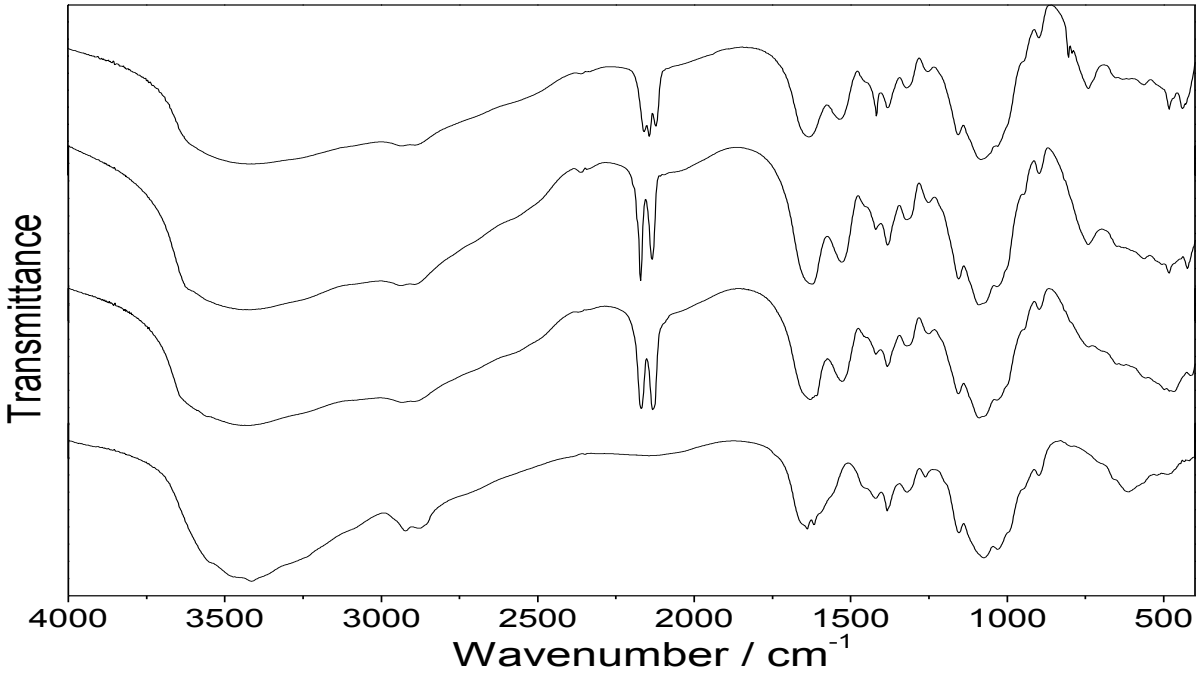

Figure S1. IR spectra of the $[Fe(pz)]^{2+}/[M(CN)_4]^{2-}$/chitosan nanocomposite beads **1** (M = Ni), **2** (M = Pd), **3** (M = Pt) and empty pristine chitosan beads from top to down.

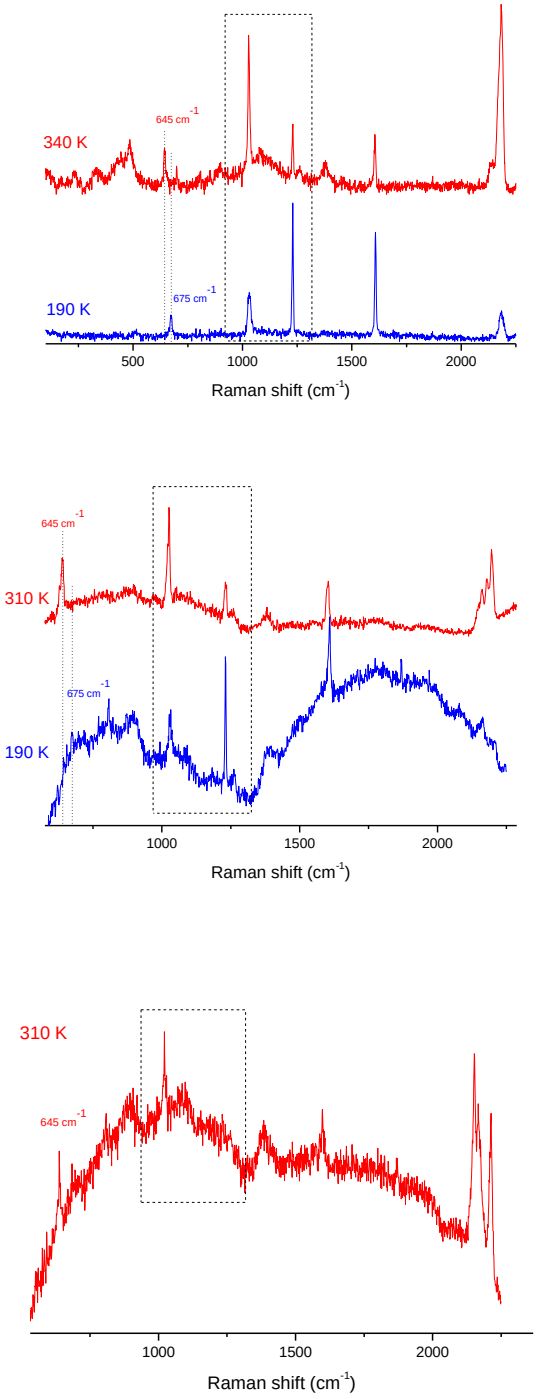

Figure S2. Raman spectra of the nanocomposite beads **1** (up), **2** (middle) and **3** (down). Variable-temperature Raman spectra were collected using a LabRAM-HR (Jobin Yvon) Raman spectrometer. The 632.8 nm line of a 17 mW He–Ne laser was used as the excitation source, and the exciting radiation was directed through a neutral density filter (OD=2) to avoid sample heating. Samples were enclosed in nitrogen atmosphere on the cold finger of a THMS600 (Linkam) liquid-nitrogen cryostage.

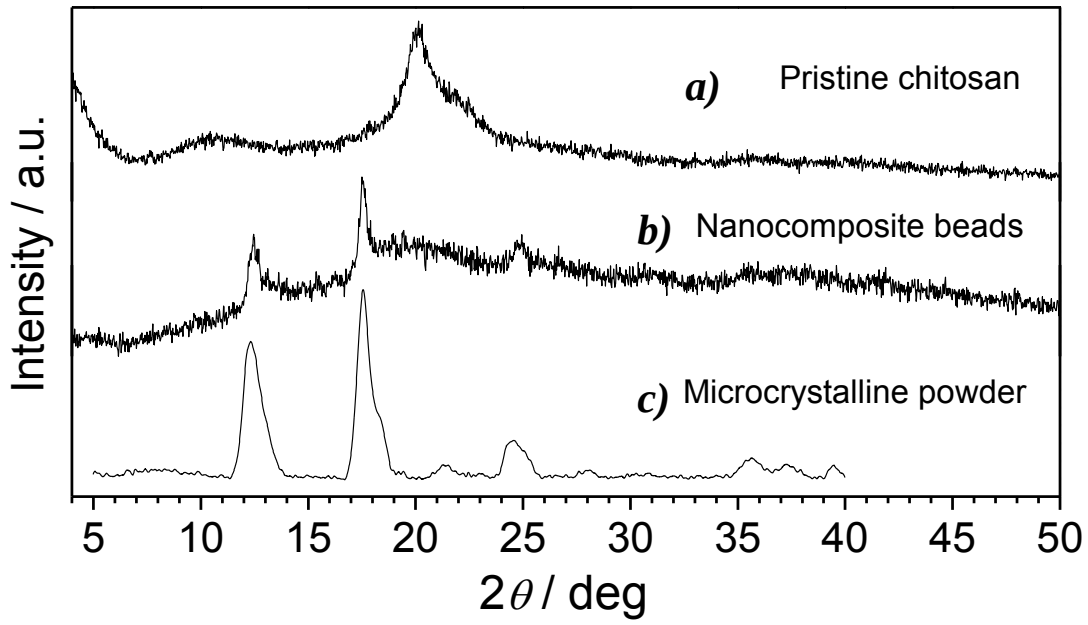

Figure S3. Powder X-ray diffraction patterns obtained for a) empty pristine chitosan beads; b) $[Fe(pz)Ni(CN)_4]$ nanocomposite beads **1**; c) $[Fe(pz)Ni(CN)_4]$ microcrystalline powder.

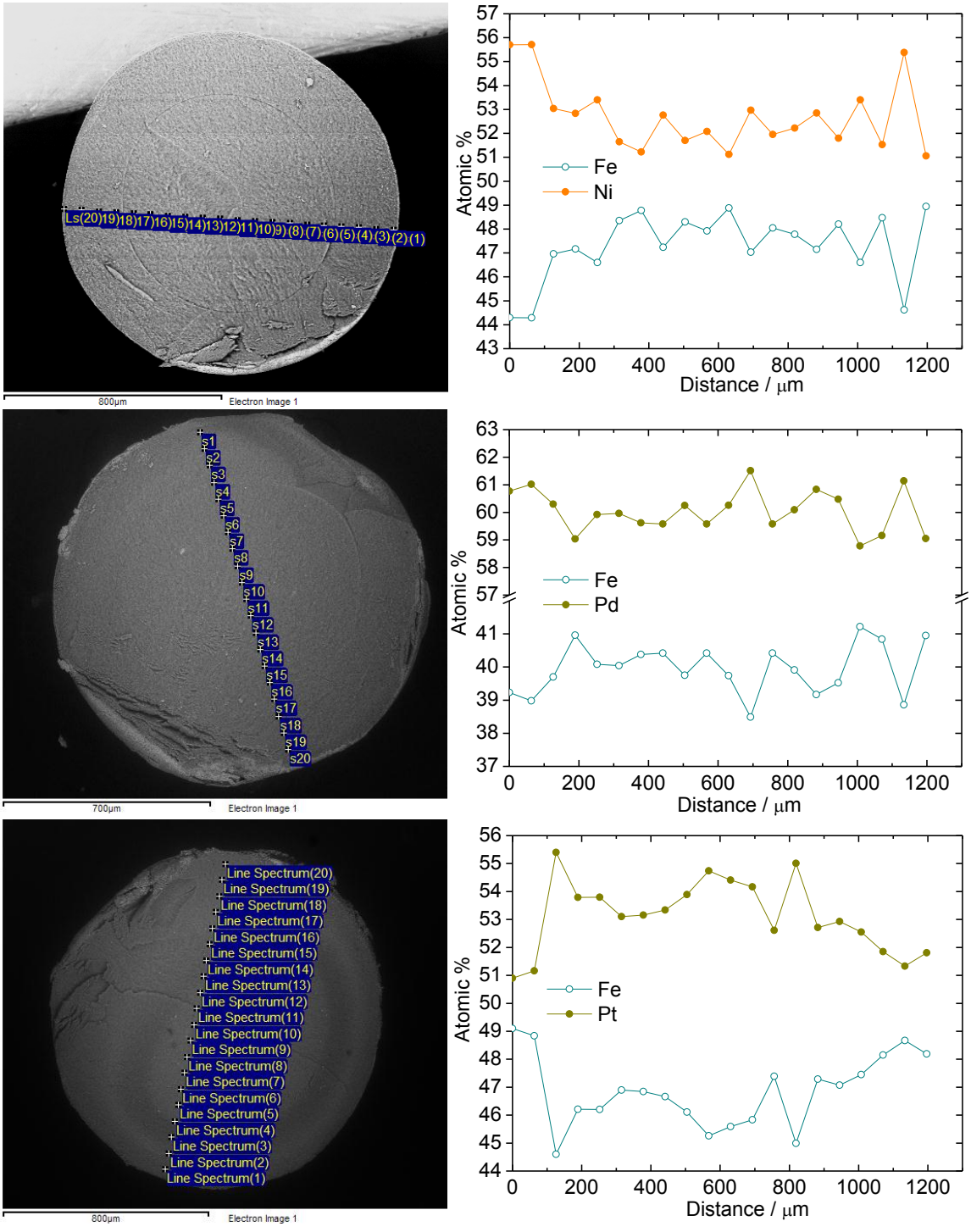

Figure S4. Internal view of the cleaved $[Fe(pz)]^{2+}/[M(CN)_4]^{2-}$/chitosan nanocomposite beads (left) and EDX profile curves (right) showing the Fe/M atomic ratio (%) versus distance (µm) for M= Ni^{2+} (top), Pd^{2+} (middle), and Pt^{2+} (bottom). The analysis includes 20 points of a record through the internal surface of the beads.

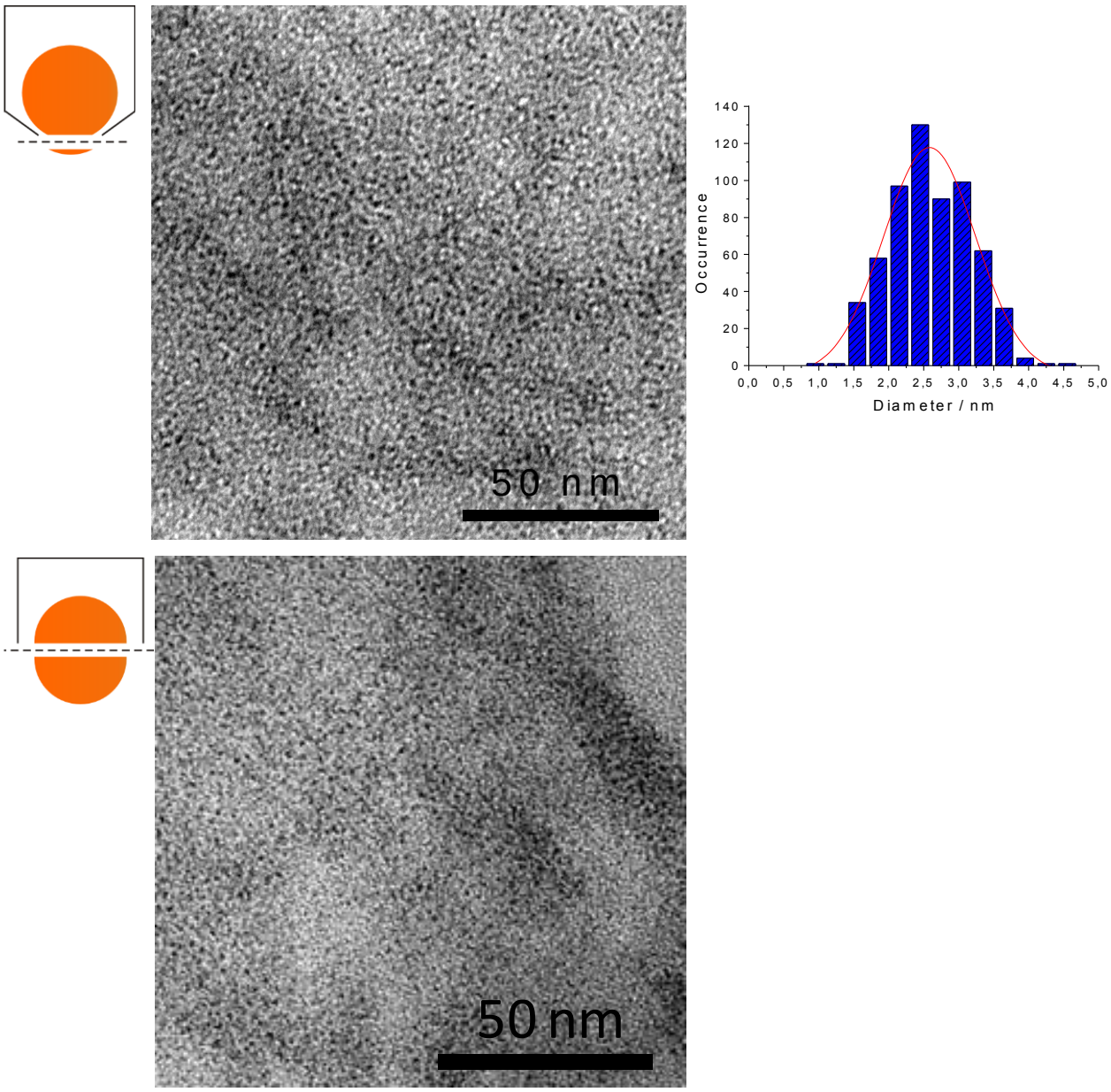

Figure S5. TEM images and size distribution of $[Fe(pz)]^{2+}/[Ni(CN)_4]^{2-}$ nanoparticles **1** obtained by ultramicrotomy from the surface (upper panel) and in the middle (lower pannel) of a chitosan bead.

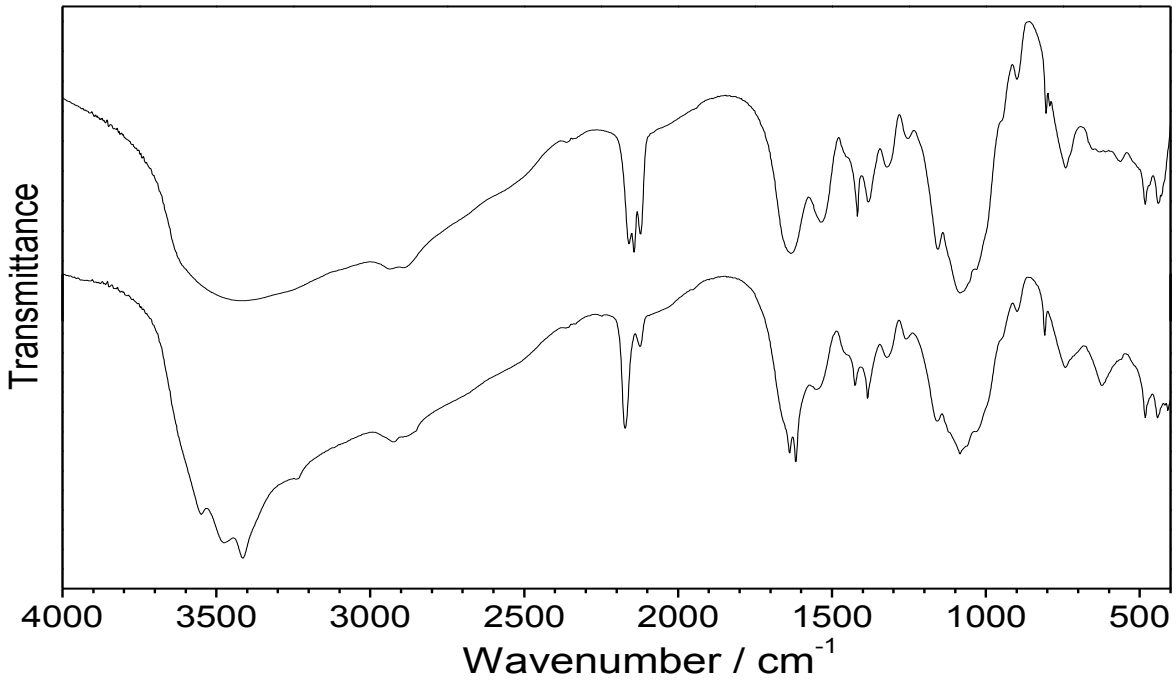

Figure S6. Comparison of the IR spectra of the nanocomposite $[Fe(pz)]^{2+}/[Ni(CN)_4]^{2-}$ /chitosan beads (**1**) (top) and $[Fe(pz)]^{2+}/[Ni(CN)_4]^{2-}$/chitosan film (**4**) obtained after solubilisation and gelation of **1** (down).

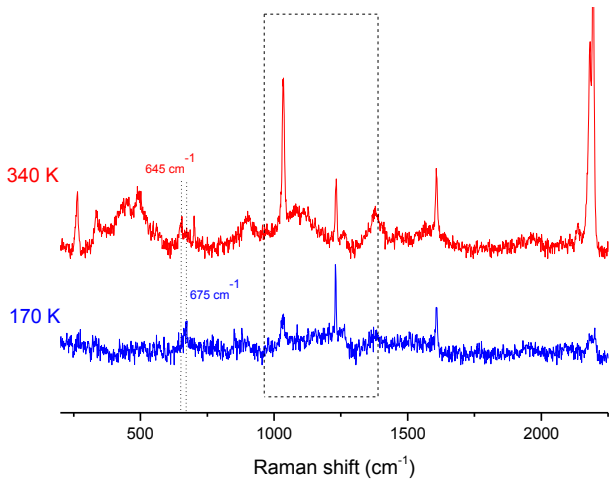

Figure S7. Raman spectra of the nanocomposite film **4** at 340 and 170 K. Variable-temperature Raman spectra were collected using a LabRAM-HR (Jobin Yvon) Raman spectrometer. The 632.8 nm line of a 17 mW He–Ne laser was used as the excitation source, and the exciting radiation was directed through a neutral density filter (OD=2) to avoid sample heating. Samples were enclosed in nitrogen atmosphere on the cold finger of a THMS600 (Linkam) liquid-nitrogen cryostage.

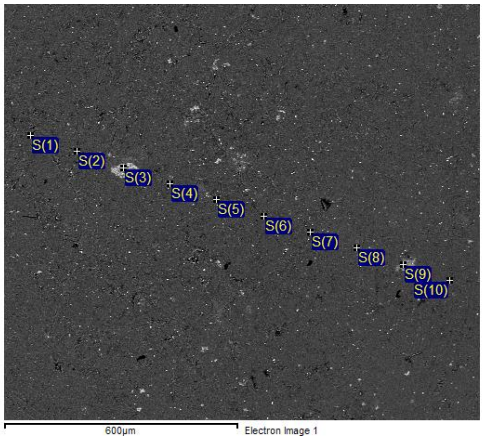

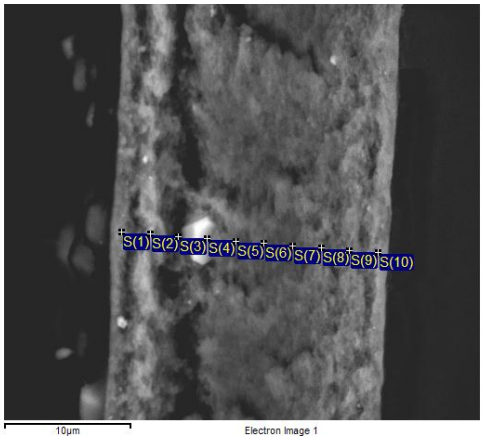

Processing option: All elements analysed (Normalised)

Spectrum	In stats.	Fe	Ni	Total
S(1)	Yes	45.04	54.96	100.00
S(2)	Yes	44.01	55.99	100.00
S(3)	Yes	46.45	53.55	100.00
S(4)	Yes	43.01	56.99	100.00
S(5)	Yes	43.37	56.63	100.00
S(6)	Yes	40.50	59.50	100.00
S(7)	Yes	43.68	56.32	100.00
S(8)	Yes	44.18	55.82	100.00
S(9)	Yes	42.15	57.85	100.00
S(10)	Yes	42.14	57.86	100.00
Mean		43.45	56.55	100.00
Std. deviation		1.66	1.66	
Max.		46.45	59.50	
Min.		40.50	53.55	

All results in weight%

Processing option: All elements analysed (Normalised)

Spectrum	In stats.	Fe	Ni
S(1)	Yes	46.28	53.72
S(2)	Yes	45.24	54.76
S(3)	Yes	47.69	52.31
S(4)	Yes	44.24	55.76
S(5)	Yes	44.61	55.39
S(6)	Yes	41.71	58.29
S(7)	Yes	44.91	55.09
S(8)	Yes	45.42	54.58
S(9)	Yes	43.38	56.62
S(10)	Yes	43.37	56.63
Mean		44.68	55.32
Std. deviation		1.67	1.67
Max.		47.69	58.29
Min.		41.71	52.31

All results in atomic%

Figure S8. (Up left) Surface and (Up right) edge views of the [[Fe(pyrazine){Ni(CN)$_4$}]/chitosan nanocomposite film **4** and EDX profile curves showing the Fe and Ni weight (%) (Down left) and atomic ratio (%) (Down right) versus distance (µm) for the edge view.

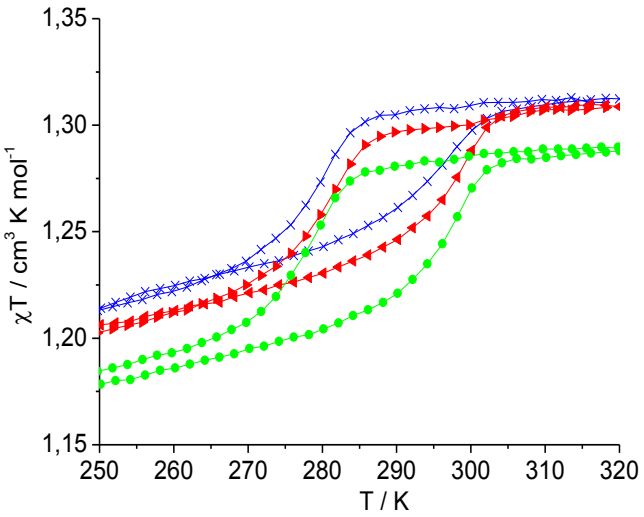

Figure S9. Temperature dependence of χT for $[Fe(pz)]^{2+}/[Pd(CN)_4]^{2-}$/chitosan nanocomposite beads recorded between 120 and 320 K at the rate of 1 K min^{-1}. The sample was isothermally held at 383 K (1 h) after 1st (-x-, blue) and 2nd (-▲-, red) cycles before the 3rd cycle (-●-, green).

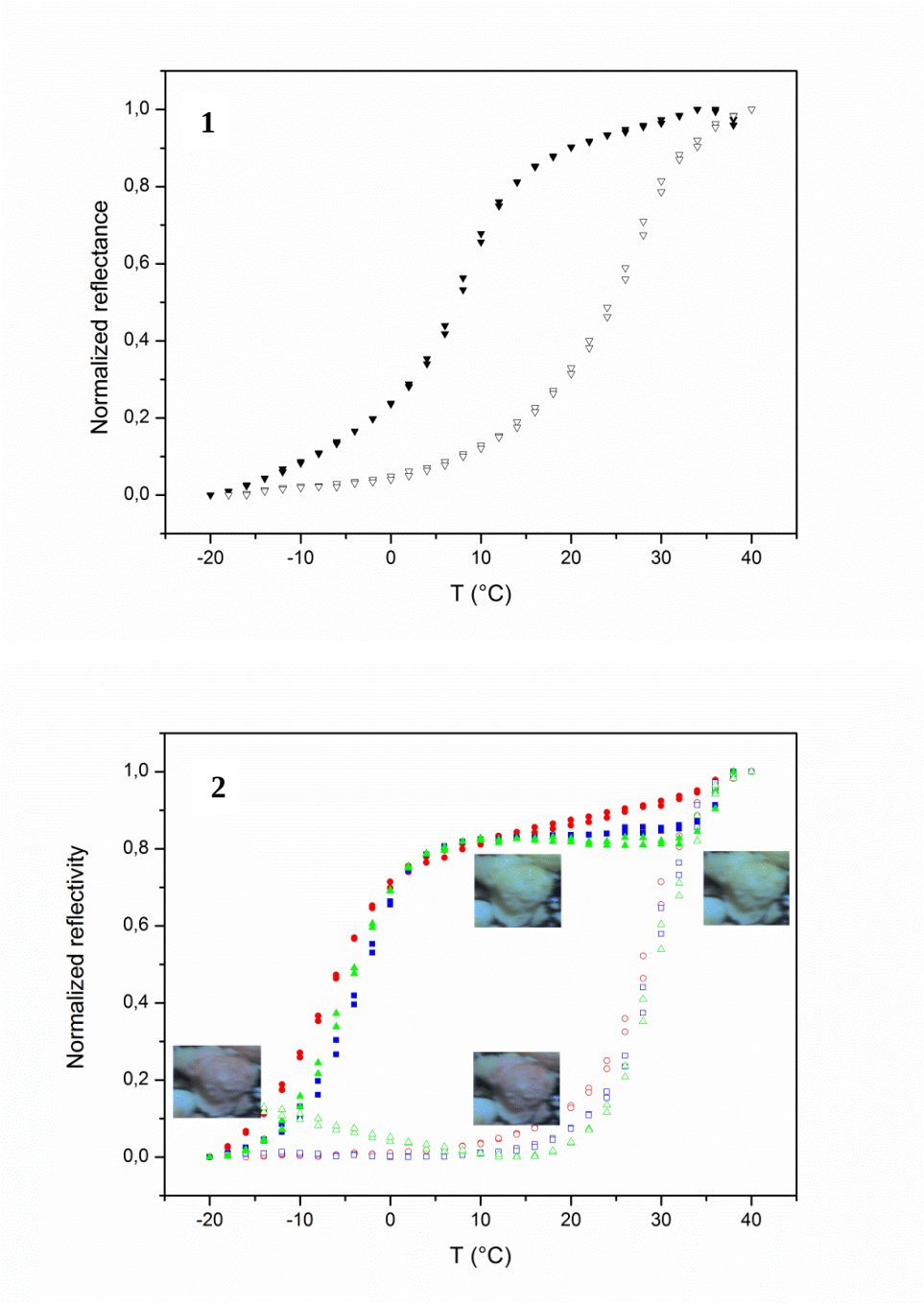

Figure S10. Thermal variation of the reflectivity for nanocomposite beads **1** (2 consecutive cycles following dehydration at 80°C in N_2 flow) and **2** (two consecutive cycles for three different sample positionsfollowing dehydration. Optical microscopy images in the inserts show the color change and the bistability centred at about 12°C.

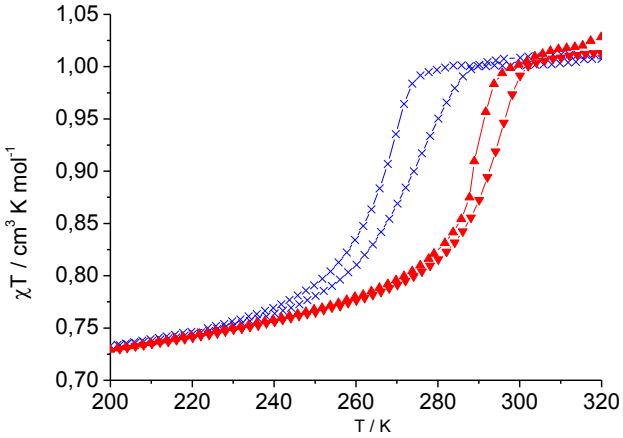

Figure S11. χT dependence *vs*. temperature for [Fe(pz){Ni(CN)$_4$}]/chitosan nanocomposite in the form of aerogel at heating and cooling rates of 1 K min^{-1}. The samples were isothermally held at 393 K during 1 h between the 1st (-X-) and 2nd (-▲-) cycle.

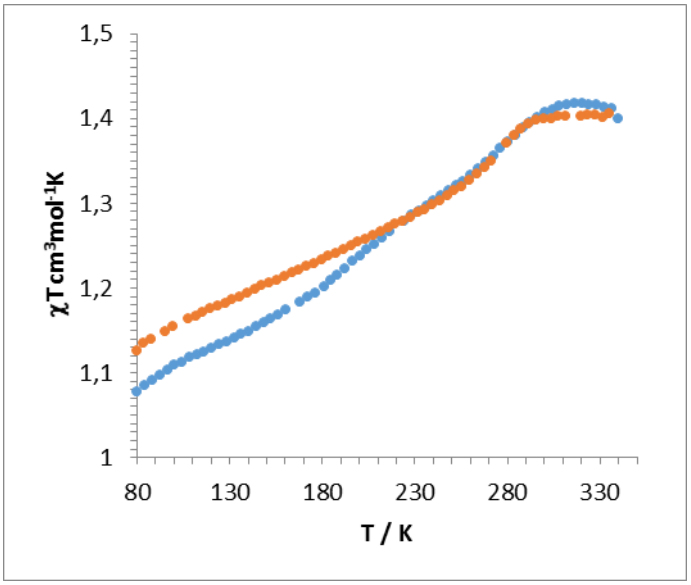

Figure S12. Thermal variation of the magnetic susceptibility for sample [Fe(pz){Ni(CN)$_4$}]/Alginate nanocomposite beads **5** (aerogel form) at heating (blue curve) and cooling (red curve) rates of 2 Kmin^{-1}

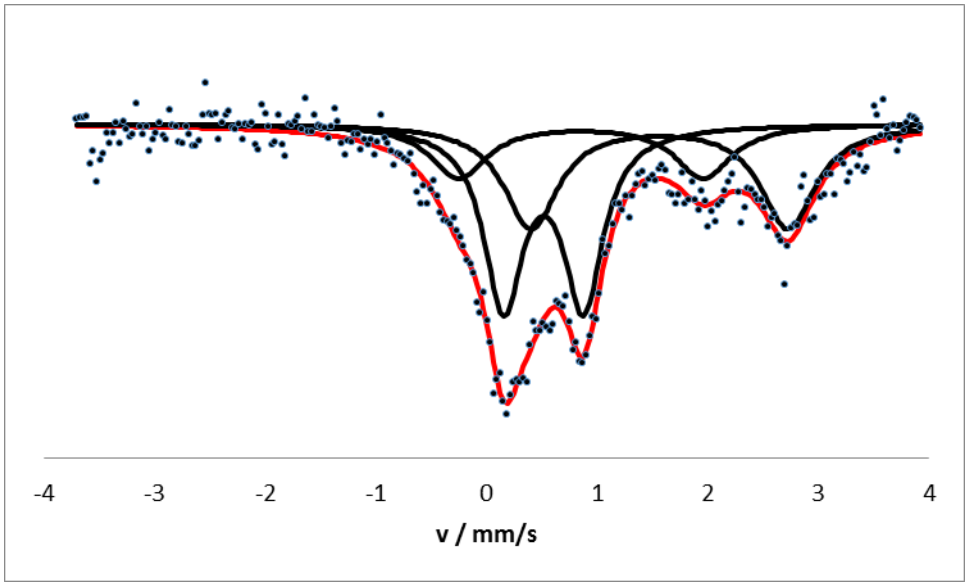

Site Parameters

	δ (mm/s)	Δ (mm/s)	Γ/2 (mm/s)
Doublet 1 HS 1	0.855(83)	2.21(14)	0.31(14)
Doublet 2 LS	1.564(44)	2.325(66)	0.299(74)
Doublet 3 HS 2	0.515(18)	0.722(34)	0.214(28)

Compiled Site Properties

	Site Populations (%)
Doublet 1 HS 1	*20(10)*
Doublet 2 LS	*36.1(92)*
Doublet 3 HS 2	*44.4(45)*

Figure S13. Mössbauer measurements for [Fe(pz){Pt(CN)$_4$}]/chitosan nanocomposite beads **3** at 80 K. The presence of at least two HS species can be inferred.

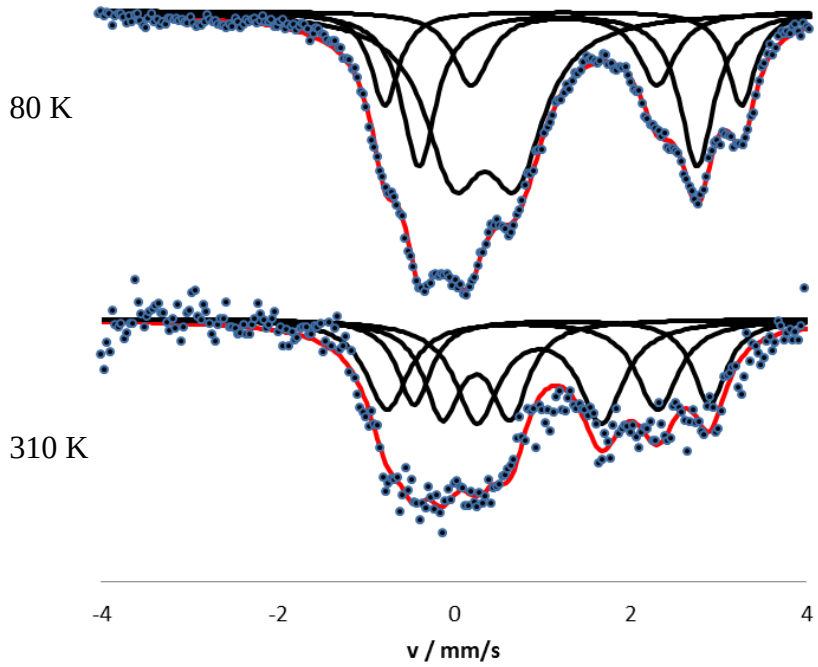

80 K

	δ (mm/s)	Δ (mm/s)	Γ/2 (mm/s)
Doublet 1	1.289(15)	1.992(38)	0.238(29)
Doublet 2	0.436(12)	0.664(24)	0.369(17)
Doublet 3	1.2238(59)	2.984(17)	0.224(22)

Site Populations (%)

Doublet 1 HS1	***14.2(27)***
Doublet 2 LS	***43.7(11)***
Doublet 3 HS2	*28.1(37)*
Doublet 4 HS3	*14.0(18)*

310 K

	δ (mm/s)	Δ (mm/s)	Γ/2 (mm/s)
Doublet 1	0.253(38)	0.766(67)	0.25*
Doublet 2	0.970(30)	1.411(73)	0.3*
Doublet 3	0.776(40)	3.070(78)	0.290(76)
Doublet 4	1.226(39)	3.356(68)	0.23*

Site Populations (%)

Doublet 1 HS1	***23.5(24)***
Doublet 2 LS	***30.4(37)***
Doublet 3 HS2	*26.3(77)*
Doublet 4 HS3	*19.8(35)*

Figure S14. Mössbauer measurements for [Fe(pz){Ni(CN)$_4$}]/Alginate nanocomposite beads **5** (aerogel form). The presence of at least three HS iron(II) species can be inferred.

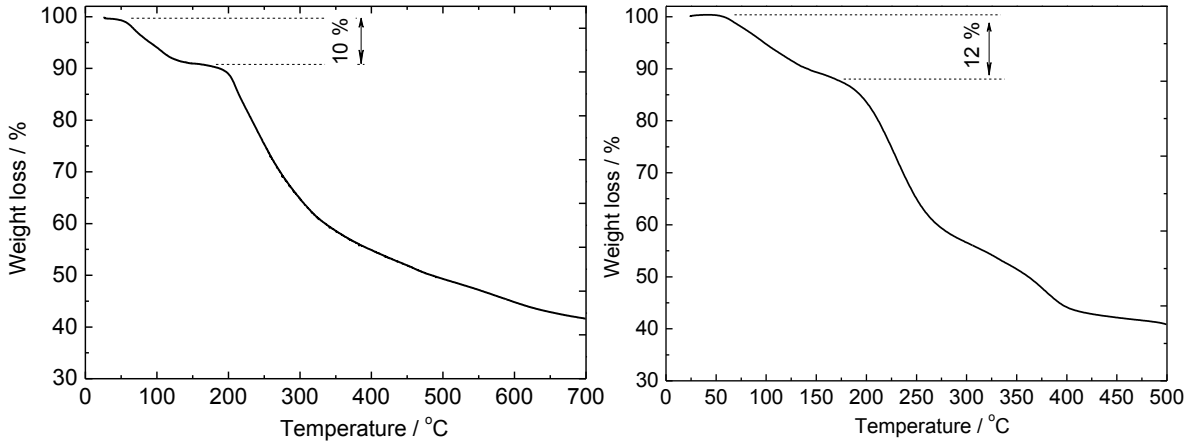

Figure S15. Thermogravimetric analyses of the $[Fe(pz)]^{2+}/[Ni(CN)_4]^{2-}$/chitosan nanocomposite beads **1** (left) and $[Fe(pz)]^{2+}/[Ni(CN)_4]^{2-}$/alginate nanocomposite beads **5** (right) obtained in nitrogen atmosphere with a rate of 2 °C/min.

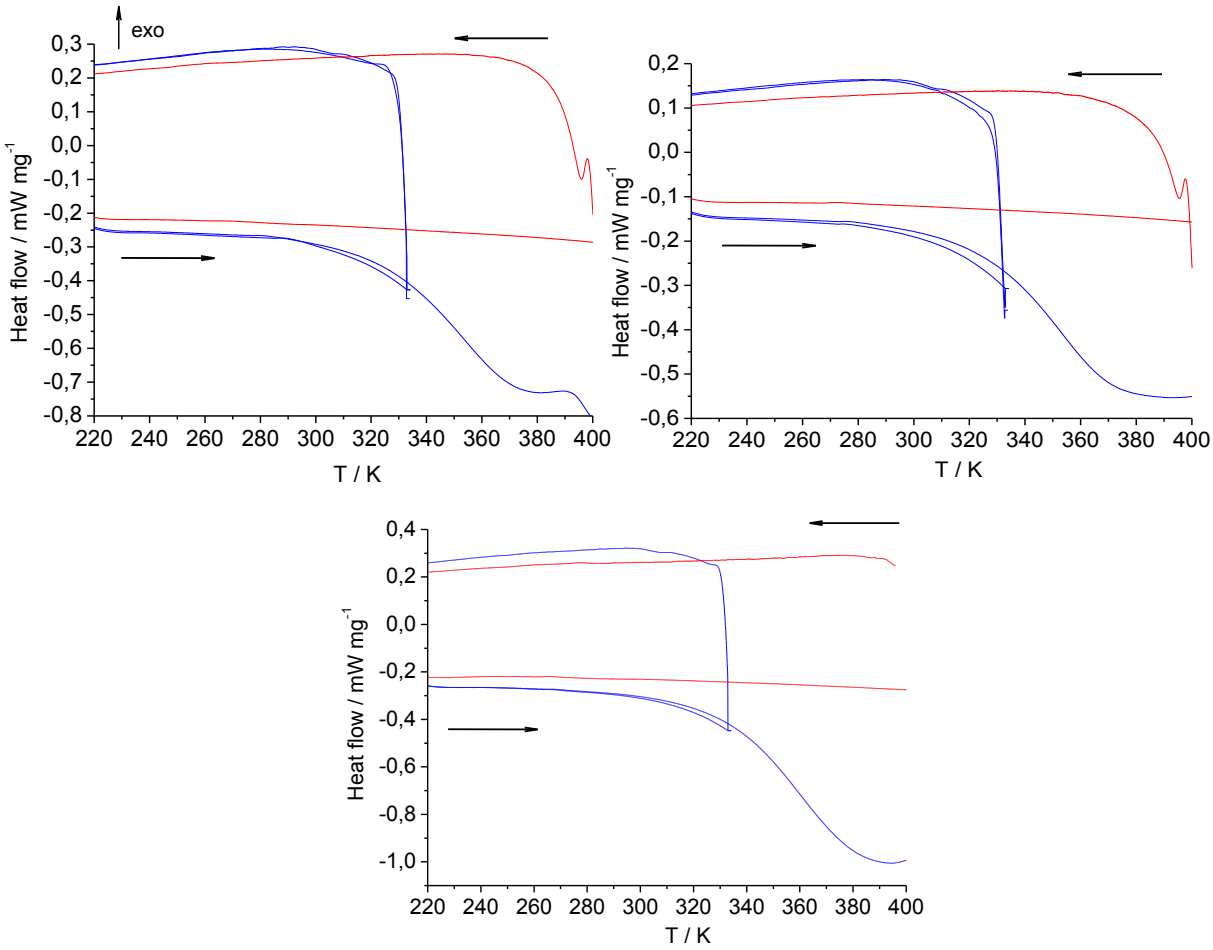

Figure S16. DSC thermograms recorded for nanocomposite **2** (left, upper panel), **3** (right, upper panel) and **5** (lower panel) in heating and cooling modes with a rate of 10 K min^{-1}: two cycles between 333↔203 K (blue), heating to 403 K with isothermal holding during 1h, and last cycle between 403↔203 K (red).